IEEE Access
Multidisciplinary ⋮ Rapid Review ⋮ Open Access Journal

Received 24 May 2024, accepted 20 July 2024, date of publication 29 July 2024, date of current version 7 August 2024.

Digital Object Identifier 10.1109/ACCESS.2024.3435051

RESEARCH ARTICLE

Low-Carbon Economic Dispatch of Integrated Energy System Considering Expanding Carbon Emission Flows

LIXIA WANG[1], HAODONG ZHAO[2], DAWEI WANG[1], FANG DONG[3], TIANMIN FENG[2], AND RUI XIONG[2]

[1]State Grid Liaoning Electric Power Supply Company Ltd., Shenyang 110000, China
[2]State Grid Shenyang Electric Power Supply Company, Shenyang 110000, China
[3]State Grid Liaoning Electric Power Research Institute, Shenyang 110000, China

Corresponding author: Lixia Wang (wanglx_2023@163.com)

This work was supported by Science and Technology Project Support of State Grid Liaoning Electric Power Company Ltd., Research on Low-Carbon Demand Response Mechanism and Benefits of Power System Based on Carbon Emission Flow Theory, under Grant 2023YF-07.

ABSTRACT To address the issues of low coordination in low-carbon operation between Carbon Capture and Storage (CCS) devices and Power to Gas (P2G) devices in integrated energy systems (IES), as well as the inaccurate characterization of carbon emissions from energy storage devices, this paper proposes an extended carbon emission flow model that integrates the collaborative operation mode of CCS-P2G and the low-carbon characteristics of energy storage. The model establishes a coupling relationship between CCS and P2G on the energy supply side to achieve low-carbon economic operation of P2G. On the energy storage side, the concept of ''electricity-carbon ratio (ECR)'' is introduced to characterize the carbon emission characteristics of energy storage devices, exploring the potential for coordinated low-carbon dispatch on both the energy supply and energy storage sides. Based on this, a low-carbon economic dispatch model for integrated energy systems is constructed, considering multiple uncertainties such as wind power, electricity prices, and electric-heat-gas loads. To achieve fast and efficient solving of the model, a parallel multi-dimensional approximate dynamic programming algorithm is adopted, which significantly improves solving efficiency by constructing a multi-layer parallel loop nested framework without losing solving accuracy. The effectiveness of the proposed model and algorithm is validated using an improved E14-H6-G6 system, consisting of a 14-node power grid, a 6-node heating network, and a 6-node gas network. The CCS-P2G (Carbon Capture, Storage, and Power-to-Gas) collaborative operation mode discussed in this article significantly enhances the economic and low-carbon performance of the Integrated Energy System (IES) by fully reutilizing CO_2. Compared to unmodified coal-fired power units, the total cost is reduced by 137,900 yuan, thereby validating the effectiveness of the CCS-P2G collaborative operation mode in low-carbon scheduling.

INDEX TERMS Low-carbon economic dispatch, carbon emission flow, CCS-P2G synergistic operation, electricity-carbon ratio, parallel multidimensional approximate dynamic programming.

I. INTRODUCTION

The clean and low-carbon transformation of energy systems is an important measure to achieve the ''dual carbon'' goals and a key element for the stable implementation of China's ''14th Five-Year Plan'' [1], [2]. However, the volatility and unpredictability of clean energy output lead to new challenges for stochastic low carbon dispatch [3], [4]. In integrated energy systems (IES) with multiple energy couplings, such as electricity, heat, and natural gas, their strong coupling characteristics and mutual conversion capabilities provide new effective pathways for accommodating new energy sources. Therefore, fully tapping into the low-carbon potential of IES across multiple stages—such as production,

The associate editor coordinating the review of this manuscript and approving it for publication was Pierluigi Siano.

transmission, conversion, and storage—is an effective means to address the unpredictability of renewable energy, promote its consumption, and enhance low-carbon dispatch decision-making [5], [6].

In response, numerous scholars both domestically and internationally have conducted research on the optimization of multi-energy-coupled integrated energy systems (IES). In the realm of electricity-gas coupling IES, literature [7] has constructed optimization scheduling models, verifying that electricity-gas coupling operation modes can enhance wind power integration capability. Furthermore, literature [8] delves into the dispatch methods of electricity-gas IES considering the potential for flexibility implied by the dynamic characteristics of natural gas operations. Regarding electricity-heat coupling IES, literature [9] proposes optimization scheduling models, demonstrating that coordinated electricity-heat operation modes can enhance system operational economy. Additionally, literature [10] further considers wind power uncertainties, validating that electricity-heat IES can effectively address uncertainties in new energy sources and improve wind power integration capability. In the realm of electricity-gas-heat coupling IES, literature [11] constructs optimization scheduling models, confirming that coordinated operation modes can enhance the economic efficiency of dispatch decisions. The aforementioned studies focus on the coupling interactions between two or three forms of energy - electricity, gas, and heat - aiming to leverage complementary advantages among multiple energy flows to enhance the economic efficiency and new energy integration capability of the system. However, they have not considered the promoting effect of power-to-gas (P2G) equipment on new energy integration. P2G equipment achieves the conversion of electricity to natural gas through processes like electrolysis of water and methanation reactions, deepening the coupling between energy sources and providing new effective pathways for new energy integration, thus drawing scholarly attention [12], [13]. Literature [14] considers P2G equipment in multi-energy-coupled IES, constructing scheduling models with the optimization of overall system economy as the goal, and verifies the effectiveness of P2G equipment in enhancing wind power integration. Nevertheless, these studies are still based on an ''electricity-centric'' perspective, constructing optimization scheduling models with the objective of minimizing operating costs, overlooking the additional costs associated with carbon emissions. This electricity-carbon separation scheduling mode to some extent restricts the low-carbon and economic operation of IES.

In response, numerous scholars both domestically and internationally have embarked on research into low-carbon dispatch in IES from a ''carbon perspective.'' Building upon the optimization of IES operations considering uncertainties, these studies also consider the impact of policies such as carbon trading mechanisms to achieve low-carbon economic operation of IES. Literature [15] introduces carbon trading mechanisms into the electricity-gas-heat IES, proving that these mechanisms can effectively promote the absorption of new energy sources and achieve low-carbon economic performance of the system. Furthermore, literature [16] incorporates source-load uncertainties into low-carbon dispatch, arguing that carbon trading mechanisms can effectively improve the low-carbon nature of systems with uncertain source-load conditions. Literature [17] considers seasonal factors in carbon trading and proposes a seasonal carbon trading mechanism based on incentive factors. However, in the aforementioned studies, high carbon-emitting coal-fired units serve as the energy supply basis, and merely establishing carbon trading mechanisms cannot fully tap into the low-carbon operational potential of IES. Therefore, carbon capture and storage (CCS) technologies applied to retrofit high-carbon-emitting units have gained favor among many scholars and have been widely used in the field of low-carbon dispatch [18], [19]. Literature [20], by retrofitting traditional coal-fired units with CCS and considering the operational flexibility of CCS units, demonstrates that CCS retrofitting of coal-fired units can effectively improve the low-carbon economic efficiency of system operation. However, most studies on CCS retrofitting technologies in the aforementioned literature are limited to single electricity systems or electricity-heat and electricity-gas coupled IES. There is a lack of quantitative analysis of the energy-saving and emission-reduction benefits brought about by CCS retrofitting in electricity-gas-heat multi-energy-coupled IES.

Furthermore, thoroughly evaluating the carbon emission flow process in low-carbon dispatching is a key criterion for assessing the efficiency of low-carbon dispatching. Consequently, the theory of carbon emission flow analysis has emerged, providing a new analytical tool for low-carbon dispatch. Literature [21] employs carbon emission flow models to examine the carbon emission data associated with energy flows, depicting the characteristics of carbon emission flow during typical dispatch periods and validating the rationality of dispatch results. However, it only indicates the path of carbon emission flow and does not analyze the precise numerical values of carbon emission flow. Literature [22], on the other hand, guides demand response by depicting the numerical values of carbon emission flow, opening up new application areas for carbon emission flow models. Nevertheless, these studies all apply carbon emission flow models without considering the integration of energy storage devices. Due to the diversity and time-coupling of energy storage device states, traditional carbon emission flow models struggle to precisely characterize the carbon emission characteristics of systems with energy storage devices. Therefore, it is urgently necessary to extend the carbon emission flow model to better integrate it into low-carbon dispatching in IES, thereby enhancing the flexibility of energy storage devices in low-carbon dispatching.

Regarding the multi-objective optimization problems in Integrated Energy Systems (IES), recent research has shown a trend towards diversification and deepening. IES, capable of integrating various energy carriers such as electricity, heat, and gas, promoting complementarity and synergy

among them, is seen as a critical component of future energy systems. However, optimizing the operation of IES encounters complexities and uncertainties, particularly when dealing with multiple conflicting objectives such as economy, environmental friendliness, and reliability, demanding that optimization models have the ability to handle multi-objective decision-making.

Considering the dynamics and uncertainties inherent in IES operations, researchers have begun to explore the combination of multi-objective optimization with advanced technologies such as machine learning and deep learning. For example, utilizing teaching-learning-based optimization to dynamically adjust the operating strategies of IES, or applying genetic algorithms to address uncertain factors, can enhance the robustness and adaptability of optimization models. In addition, literature [23] improved the Approximate Dynamic Programming (ADP) algorithm based on multi-parametric programming theory, developing a stable energy management algorithm based on Multi-Agent Dynamic Programming (MADP).

However, MADP algorithms face challenges such as state space explosion, high computational complexity, difficulties in information sharing, and the design of cooperative strategies, requiring substantial computational resources and thus are only applicable to small-scale problems.

To address the aforementioned issues, this paper introduces the concept of CCS-P2G synergistic operation mode and extended carbon emission flow, proposing a CCS-P2G-energy storage (ES) coordinated low-carbon dispatch model. The main contributions are as follows:

1) The paper proposes the CCS-P2G synergistic operation mode, constructing an integrated operational framework for carbon emission ''generation-capture-utilization''. This mode resolves the low economic efficiency issue of P2G devices due to high raw material costs, thereby enhancing the operational economy of IES.
2) The concept of electricity-carbon ratio (ECR) is introduced to precisely characterize the carbon emission characteristics of electric energy storage devices. It considers the impact of their charging and discharging states on the carbon emission flow of the entire network and integrates the dynamic relationship between carbon emissions and electricity in electric energy storage devices over the entire dispatch cycle. This achieves uniform carbon emission flow models for various devices in IES, further improving the accuracy of low-carbon dispatch in IES.
3) An extended carbon emission flow model considering electric energy storage devices is proposed. By combining ECR with traditional carbon emission flow models, the model aligns with IES containing energy storage, accurately describing the carbon emission flow path of the process of sources-network-loads-storage. This effectively broadens the application range of carbon emission flow models, providing new criteria for assessing the rationality and effectiveness of low-carbon dispatch strategies in IES.

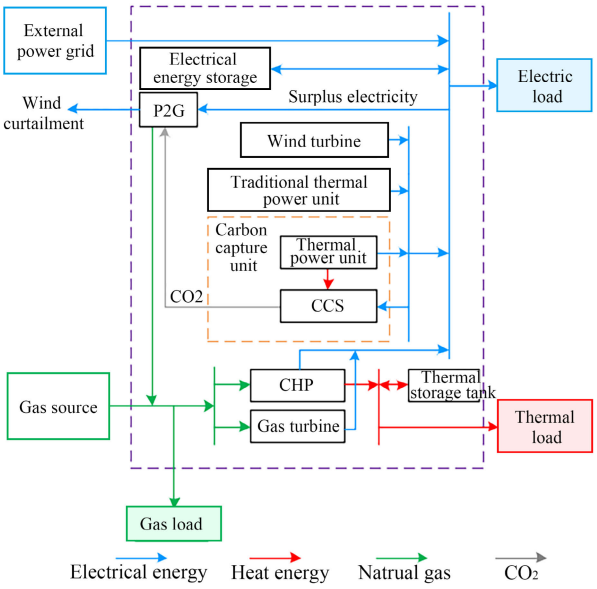

FIGURE 1. Basic structure of IES with CCS-P2G.

II. THE SYNERGISTIC OPERATION OF CCS AND P2G IN IES

A. COMPONENTS OF IES

The high carbon emissions from traditional coal-fired power units pose challenges to the low-carbon operation of IES. This paper couples CCS with P2G to form a CCS-P2G synergistic operation system, capturing a large amount of CO_2 emitted by traditional coal-fired power units through CCS and providing sufficient carbon feedstock for P2G. The architecture of IES considering the synergistic operation of CCS-P2G is illustrated in Fig.1.

From Fig.1, it can be seen that the electrical system in the Integrated Energy System (IES) includes traditional coal-fired power units without low-carbon transformation, carbon capture units composed of CCS and some coal-fired power units, electrical energy storage devices, wind turbines, external power grids, and electrical loads. The thermal system consists of thermal storage tanks and thermal loads, while the natural gas system comprises gas sources and gas loads. Energy coupling equipment includes P2G, combined heat and power (CHP), and gas turbines. Excess electrical energy in the system is directed towards P2G, where it is converted into natural gas to supply gas loads. Some of the natural gas is directed towards gas turbines to convert into electricity to supply electrical energy storage devices and electrical loads, while some is directed towards CHP to convert into electricity and heat, supplying electrical energy storage devices, electrical loads, and thermal storage tanks and thermal loads respectively.

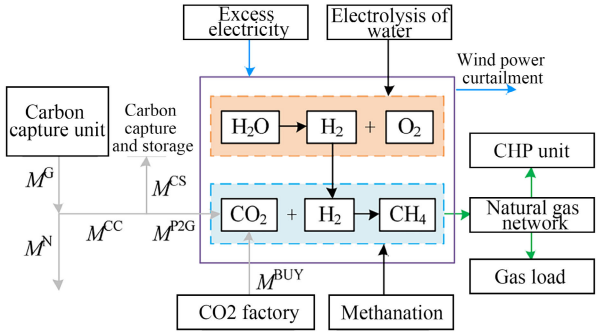

FIGURE 2. CCS-P2G collaborative operation mode.

B. CCS-P2G COLLABORATIVE OPERATION MODE

The collaborative operation mode of CCS-P2G as shown in Fig.2. M^G represents the total amount of CO_2 emitted by the carbon capture unit; M^{CC} represents the amount of CO_2 captured by CCS; M^N represents the amount of CO_2 emitted into the air by the carbon capture unit, which is the difference between M^G and M^{CC}; M^{CS} represents the amount of CO_2 sequestered in the CCS capture; M^{P2G} represents the amount of CO_2 captured by CCS supplied for P2G utilization; M^{BUY} represents the amount of CO_2 purchased by the P2G from external CO_2 factories.

From Fig.2, it can be observed that P2G achieves the conversion of electrical energy to natural gas energy through two processes: electrolysis of water and methanation. Firstly, P2G produces H_2 and O_2 through the electrolysis of water. Secondly, utilizing CO_2 captured by CCS from coal-fired power plants and H_2 generated during the electrolysis process, CH_4 is produced through methanation. The collaborative operation mode of CCS-P2G not only reduces the carbon emissions from traditional coal-fired power plants but also fully utilizes CO_2 within the system, thereby reducing the cost of external CO_2 purchase for P2G and improving the low-carbon economic viability of IES.

III. EXTENDED CARBON EMISSION FLOW MODEL CONSIDERING ENERGY STORAGE

Based on the theory of carbon emission flow, this paper assumes that CO_2 generated at the source is not directly emitted into the atmosphere. Instead, it is transferred to the load side via power line flows, creating a virtual ''carbon flow'' associated with the line flows. This ''carbon flow'' can intuitively represent the direction of carbon emissions during system operation, providing a new analytical perspective for low-carbon economic dispatch.

A. CARBON EMISSION FLOW MODEL FOR NETWORK AND ENERGY-COUPLING EQUIPMENT

1) NETWORK CARBON EMISSION FLOW MODEL

This paper is based on the theories presented in references [24] and [25] to establish the key elements and construction methods of the carbon emission flow model.

a: CARBON EMISSION FLOW RATE

The carbon emission flow rate (CEFR) is used to define the amount of carbon emissions passing through network branches or nodes within a unit of time (measured in tCO_2/h).

$$f^{CEFR} = dF/dt \tag{1}$$

where f^{CEFR} represents the carbon emission flow rate; F represents the amount of carbon emissions passing through network branches or nodes; t represents time.

b: CARBON EMISSION INTENSITY

Carbon emission intensity (CI) is the amount of carbon emissions associated with unit energy (measured in $tCO_2/(MW{\cdot}h)$. CI is typically divided into several types: generation carbon intensity (GCI), branch carbon intensity (BCI), port carbon intensity (PCI), and node carbon intensity (NCI). GCI represents the amount of carbon emissions per unit of energy generated at the source. BCI represents the amount of carbon emissions per unit of energy flowing along a branch. PCI represents the amount of carbon emissions associated with the input or output energy of energy-coupling equipment. NCI reflects the cumulative effect of carbon emission intensity. The carbon emission intensities of various branches connected to the same node are mixed and summed at the node, representing the average carbon emission per unit of energy injected into the node. Mathematically, NCI for node n in time period t is represented by Equation (2).

$$f_{i,t}^{\mathrm{NCI},e} = \frac{\sum_{b^e.\in i^+} f_{b^e,t}^{e} f_{b^e,t}^{\mathrm{BCI},e} + \sum_{g.\in i} P_{g,t} f_{g,t}^{\mathrm{GCI},e}}{\sum_{b^e.\in i^+} f_{b^e,t}^{e} + \sum_{g.\in i} P_{g,t}} \tag{2}$$

where $f_{i,t}^{\mathrm{NCI},e}$, $f_{b^e,t}^{\mathrm{BCI},e}$, $f_{g,t}^{\mathrm{GCI}}$ represent the carbon emission intensity of node i, branch b^e, and generator g in time period t, respectively; $b^e. \in i^+$ represents branch b^e with node i as the starting node; $g \in i$ represents generator g connected to node i; $f_{b^e,t}^{e}$ represents the electrical power flow through branch b^e in time period t; $P_{g,t}$ represents the power of generator g in time period t.

Thus far, this paper has constructed a carbon emission flow model for the power grid, mapping carbon flow to the corresponding power flow. This gives the previously virtual carbon emission flow process a clear physical meaning. Moreover, by only injecting the power flow at nodes and GCI, the distribution of carbon emissions flow across the entire network can be calculated, making the calculation simple and practical.

In addition to the carbon emission flow model in the power network, this paper, referencing literature [26], provides methods for constructing carbon emission flow models for thermal and natural gas networks, as shown in Equations (F1) and (F2) in Appendix F.

2) CARBON EMISSION FLOW MODEL FOR ENERGY-COUPLING EQUIPMENT

When converting different types of energy, carbon emissions also transfer among various energy systems. By construct-

ing a carbon emission flow model for energy-coupling equipment, it is possible to examine the carbon emission transfer characteristics during energy transfer, thus establishing a better carbon emission flow model. Reference [26] categorizes energy-coupling equipment into single-input-single-output devices (such as gas turbines, P2G) and single-input-multiple-output devices (such as CHP), and has established their respective carbon emission flow models. This paper adopts a similar modeling approach, with detailed modeling procedures outlined in Appendix D.

B. CARBON EMISSION FLOW MODEL FOR ENERGY STORAGE DEVICES

In IES, devices are typically categorized into three types based on their energy utilization: energy-discharging devices, such as power generation units; energy-consuming devices, such as various loads; and energy-coupling devices, such as P2G. Energy storage devices have both discharging and charging states. When in the discharging state, energy storage devices act as special loads and can absorb some carbon emissions; when in the charging state, they act as special power generation devices and release some carbon emissions. The multi-state nature of energy storage devices increases the complexity of their carbon emission flow models. Therefore, this paper refers to the state of charge (SOC) of electric energy storage devices and proposes the concept of Electric Energy Storage Carbon Relationship (ECR) to characterize the relationship between the electric energy and the absorbed carbon emissions in electric energy storage devices.

When electric energy storage devices are in the charging state, carbon emissions are associated with the charging of electric energy into the devices:

$$M_{e,t}^{cha} = P_{e,t}^{cha} f_{e,t}^{\mathrm{NCl}} \Delta t \tag{3}$$

where $M_{e,t}^{cha}$ represents the carbon emissions absorbed by electric energy storage device e during time period t when charging; $P_{e,t}^{cha}$ represents the charging power of electric energy storage device e during time period t; $f_{e,t}^{\mathrm{NCl}}$ represents the NCI of the node where electric energy storage device e is located during time period t, calculated using Equation (2) by treating the electric energy storage device as a load; Δt is the time interval.

When the electric energy storage device is in the discharging state, carbon emissions are released externally along with the discharge of electricity from the device.

$$M_{e,t}^{\mathrm{dis}} = P_{e,t}^{\mathrm{dis}} f_{e,t}^{\mathrm{GCl}} \Delta t = \frac{P_{e,t}^{\mathrm{dis}}}{\eta_e^{\mathrm{dis}}} f_{e,t-1}^{\mathrm{ECR}} \Delta t \tag{4}$$

where $M_{e,t}^{\mathrm{dis}}$ represents the carbon emissions released by electric energy storage device e during time period t; $P_{e,t}^{\mathrm{dis}}$ represents the discharging power of electric energy storage device e during time period t; $f_{e,t}^{\mathrm{GCl}}$ represents the GCI of electric energy storage device e when acting as a power generation device during time period t; η_e^{dis} represents the discharging efficiency of electric energy storage device e; $f_{e,t-1}^{\mathrm{ECR}}$ represents the ECR of electric energy storage device e during time period t-1.

The ECR of the electric energy storage device is defined as:

$$f_{e,t}^{\mathrm{ECR}} = \frac{f_{e,t-1}^{\mathrm{ECR}} E_{e,t-1} + M_{e,t}^{\mathrm{cha}} - M_{e,t}^{\mathrm{dis}}}{E_{e,t}} \tag{5}$$

where $E_{e,t}$ represents the available capacity of electric energy storage device e during time period t.

In summary, by mapping the energy storage and release process to the carbon emission storage and release process, a unified carbon emission flow model for each component in the Integrated Energy System (IES) considering energy storage devices has been constructed, thereby broadening the application scope of the carbon emission flow model.

IV. IES LOW-CARBON ECONOMIC DISPATCH MODEL

This paper constructs an IES low-carbon economic dispatch model and utilizes the parallel multi-dimensional approximate dynamic programming (PMADP) algorithm [27] for solving.

A. OBJECTIVE FUNCTION

The objective of stochastic dynamic low-carbon dispatch in IES is to optimize the overall low-carbon economic efficiency while satisfying the constraints of the power system (PS), heat system (HS), and natural gas system (NGS). This paper integrates the operating costs of CHP and gas turbines into the unified calculation of purchased natural gas costs [28].

$$F = \mathbb{E}\{F_n\}, n \in N \tag{6}$$

$$F_n = \min\left\{\sum\left(f_{n,t}^{\mathrm{e}} + f_{n,t}^{\mathrm{h}} + f_{n,t}^{\mathrm{g}}\right) + f_n^{\mathrm{c}}\right\}, n \in N \tag{7}$$

where F represents objective function, F_n represents the total operating cost of scenario n; $f_{n,t}^{\mathrm{e}}$, $f_{n,t}^{\mathrm{h}}$ and $f_{n,t}^{\mathrm{g}}$ are the operating costs of PS, HS, and NGS, respectively, in time period t of scenario n; f_n^{c} is the carbon trading cost for the entire scheduling cycle; N is the set of scenarios.

1) CARBON TRADING COST

The carbon trading cost f_n^c is usually calculated on a "daily" time scale. This paper adopts the method of calculating the carbon trading cost for the entire scheduling cycle, which consists of CO_2 transportation and storage cost $f_n^{c,trans}$, carbon quota excess cost $f_n^{c,cost}$, and purchased CO_2 cost $f_n^{c,buy}$ for P2G [29].

$$f_n^c = f_n^{\mathrm{c,\,trans}} + f_n^{\mathrm{c,\,cost}} + f_n^{\mathrm{c,\,buy}} \tag{8}$$

where

$$\begin{cases} f_n^{\text{c, trans}} = C^{\text{c, trans}} \left(\sum_{t\in T} \sum_{k\in K} M_{k,n,t}^{\text{ccs}} - \sum_{t\in T} \sum_{u\in U} M_{u,n,t}^{\text{p2g}} \right) \\ f_n^{\text{c,cost}} = C^{\text{c, deal}} \left(M_{n,t}^{\text{all}} - \sum_{t\in T} \sum_{g\in G} \lambda_g^{\text{CO}_2} P_{g,n,t} \right. \\ \quad - \sum_{t\in T} \sum_{k\in K} \lambda_k^{\text{CO}_2} P_{k,n,t} \\ \quad - \sum_{t\in T} \sum_{c\in C} \lambda_c^{\text{CO}_2} \left(P_{c,n,t} + H_{c,n,t} \right) \\ \quad \left. - \sum_{t\in T} \sum_{r\in R} \lambda_r^{\text{CO}_2} P_{r,n,t} - \sum_{t\in T} \sum_{o\in O} \lambda_o^{\text{CO}_2} P_{o,n,t} \right) \\ f_n^{\text{c,buy}} = C^{\text{buy,CO}_2} \left(\sum_{t\in T} \sum_{u\in U} \tau_u^{\text{CO}_2} P_{u,n,t} - \sum_{t\in T} \sum_{k\in K} M_{k,n,t}^{\text{css}} \right) \end{cases} \tag{9}$$

where $C^{\text{c, trans}}$, $C^{\text{c, deal}}$ and $C^{\text{buy,CO}_2}$ are the coefficients for CO_2 transportation and storage, trading, and purchasing costs respectively; $M_{k,n,t}^{\text{ccs}}$ is the amount of CO_2 captured by coal-fired unit k with CCS in time period t in scenario n; $M_{u,n,t}^{\text{p2g}}$ is the amount of CO_2 consumed by P2G unit u in time period t in scenario n; $M_{n,t}^{\text{all}}$ is the total amount of CO_2 generated by IES in time period t in scenario n; $\lambda_g^{\text{CO}_2}$, $\lambda_k^{\text{CO}_2}$, $\lambda_c^{\text{CO}_2}$ and $\lambda_r^{\text{CO}_2}$ represent the carbon emission quota coefficients for coal-fired unit g, coal-fired unit k with CCS, CHP unit c, and gas turbine unit r, respectively; $\lambda_o^{\text{CO}_2}$ is the carbon emission quota coefficient for external power grid o; $P_{g,n,t}$, $P_{k,n,t}$, $P_{c,n,t}$, $P_{r,n,t}$ are the output of coal-fired unit g, coal-fired unit k with CCS, CHP unit c, and gas turbine unit r in time period t in scenario n, respectively; $P_{o,n,t}$ is the purchased power from external power grid o in scenario n; $H_{c,n,t}$ is the thermal output of CHP unit c in time period t in scenario n; $\tau_u^{\text{CO}_2}$ is the amount of CO_2 consumed to produce electricity by P2G generation units; $P_{u,n,t}$ is the energy consumption of P2G device u in scenario n; K, U, G, C, R, and O respectively represent the sets of coal-fired units with CCS, P2G devices, coal-fired units, CHP units, gas turbines, and external power grids; T represents the set of scheduling periods.

2) PS OPERATING COST

$$\begin{aligned} f_{n,t}^{\text{e}} = & \sum_{g\in G} C_g P_{g,n,t} + \sum_{r\in R} C_r P_{r,n,t} + \sum_{o\in O} p_{n,t} P_{o,n,t} \\ & + \sum_{i\in I} C^{\text{np}} P_{i,n,t}^{\text{np}} + \sum_{e\in E} \left(C_e^{\text{cha}} P_{e,n,t}^{\text{cha}} + C_e^{\text{dis}} P_{e,n,t}^{\text{dis}} \right) \\ & + \sum_{w\in W} C^{\text{nw}} P_{w,n,t}^{\text{nw}}, \ \forall n \in N, \ \forall t \in T \end{aligned} \tag{10}$$

$$P_{w,n,t}^{\text{nw}} = \max \left(P_{w,n,t}^{\text{f}} - P_{w,n,t}, 0 \right), \quad \forall n \in N, \ \forall t \in T \tag{11}$$

where C_g and C_r are the operating cost coefficients for coal-fired unit g and gas turbine r, respectively; C_e^{cha} and C_e^{dis} are the charging cost coefficient and discharging cost coefficient for energy storage equipment e, respectively; C^{np} and C^{nw} are the penalty coefficients for load shedding and wind curtailment, respectively; $p_{n,t}$ is the electricity price in period t for scenario n; $P_{i,n,t}^{\text{np}}$ is the load shedding power at node i in period t for scenario n; $P_{w,n,t}^{\text{nw}}$ is the wind curtailment power in period t for scenario n; $P_{w,n,t}^{\text{f}}$ is the wind power forecast in period t for scenario n; $P_{w,n,t}$ is the actual wind power consumption in period t for scenario n; I is the set of all nodes; W is the set of wind power units.

3) HS OPERATING COST

$$f_{n,t}^{h} = \sum_{z\in Z} C^{\text{nsh}} H_{z,n,t}^{\text{nsh}}, \quad \forall n \in N, \ \forall t \in T \tag{12}$$

where C^{nsh} is the penalty coefficient for heat load shedding; $H_{z,n,t}^{\text{nsh}}$ is the amount of heat load shedding at thermal network node z in period t for scenario n; Z is the set of thermal network nodes.

4) NGS OPERATION COST

$$f_{n,t}^{\text{g}} = \sum_{s\in S} C_s G_{s,n,t} + \sum_{m\in M} C^{\text{nsg}} G_{m,n,t}^{\text{nsg}}, \quad \forall n \in N, \ \forall t \in T \tag{13}$$

where C_s is the cost of natural gas source s; C^{nsg} is the penalty coefficient for natural gas load shedding; $G_{m,n,t}^{\text{nsg}}$ is the amount of gas load shedding at gas network node m in period t for scenario n; $G_{s,n,t}$ is the amount of natural gas output from source s in period t for scenario n; S is the set of natural gas sources; M is the set of gas network nodes.

B. CONSTRAINT CONDITIONS

The constraint conditions of the IES stochastic dynamic low-carbon dispatch model include: power system constraints, thermal system constraints, natural gas system constraints, and energy coupling device constraints.

1) POWER SYSTEM CONSTRAINTS

These mainly include power balance constraints, constraints on the operation of coal-fired units with CCS, line flow constraints, unit operation limits, and ramping constraints. For details on power system constraints, refer to Appendix E. Additionally, since the expanded carbon emission flow model proposed in this paper can be widely applied in IES day-ahead or intraday scheduling, it is suitable for both intraday scheduling with known unit start-up and shutdown states, and IES scheduling considering unit start-up and shutdown decisions for the day-ahead. Therefore, the power system constraints considered in this paper do not currently include unit start-up and shutdown decisions.

2) THERMAL SYSTEM CONSTRAINTS

A typical thermal system includes thermal stations, thermal network pipelines, and heat exchanger stations, with thermal

stations acting as heat sources and heat exchanger stations acting as heat loads. In deterministic scenario n, thermal system constraints include constraints on the operation of thermal stations, thermal network constraints, and constraints on the operation of heat exchanger stations. For details on thermal system constraints, refer to Reference [27], and specific details are not reiterated here.

3) NATURAL GAS SYSTEM CONSTRAINTS

In deterministic scenarion, natural gas system constraints include constraints on natural gas network node flow balance, constraints on natural gas network pipeline operations, and model transformation constraints. References [28] provide details on natural gas system constraints.

a: CONSTRAINTS ON NATURAL GAS NETWORK NODE FLOW BALANCE

$$\sum_{s\in a} G_{s,n,t} + \sum_{u.\in a} G_{u,n,t} + \sum_{a.\in(\cdot,b)} G_{ab,n,t} - \sum_{a\in(b,\cdot)} G_{ba,n,t} + G^{\mathrm{ng}}_{a,n,t} = G_{a,n,t} + \sum_{c.\in a} G_{c,n,t} + \sum_{r.\in a} G_{r,n,t}, \quad \forall s \in S,\ \forall a \in A,\ \forall c \in C,\ \forall r \in R \tag{14}$$

where . $\in a$ the connection to the natural gas network node a; $G_{s,n,t}$ is the output of natural gas source s in period t for scenario n; $G_{u,n,t}$ represents the gas production of P2G device u in scenario n during time period t; $G_{ab,n,t}$ represents the gas flow in pipeline ab of the natural gas network in scenario n during time period t; $G^{g,n}_{a,n,t}$ represents the gas shedding load at node a of the natural gas network in scenario n during time period t; $G_{a,n,t}$ represents the predicted gas load at node a of the natural gas network in scenario n during time period t; $G_{c,n,t}$ represents the gas consumption of CHP unit c in scenario n during time period t; $G_{r,n,t}$ represents the gas consumption of gas turbine r in scenario n during time period t; A represents the set of nodes in the natural gas network.

b: OPERATIONAL CONSTRAINTS OF NATURAL GAS NETWORK PIPELINES

$$G^2_{ab,n,t} = \left(\frac{\pi}{4}\right)^2 J_{ab}\left(p^2_{a,n,t} - p^2_{b,n,t}\right), \quad \forall n \in N,\ \forall t \in T \tag{15}$$

$$G^{\min}_{ab} \le G_{ab,n,t} \le G^{\max}_{ab}, \quad \forall n \in N,\ \forall t \in T \tag{16}$$

$$p^{\min}_{a} \le p_{a,n,t} \le p^{\max}_{a}, \quad \forall n \in N,\ \forall t \in T \tag{17}$$

$$p^{\min}_{b} \le p_{b,n,t} \le p^{\max}_{b}, \quad \forall n \in N,\ \forall t \in T \tag{18}$$

where J_{ab} represents the physical coefficient of pipeline ab in the natural gas network; $P_{a,n,t}$ and $P_{b,n,t}$ represent the pressure at nodes a and b in the natural gas network in scenario n during time period t, respectively; $G^{\max}_{ab}$ and $G^{\min}_{ab}$ represent the upper and lower limits of the gas flow in pipeline ab of the natural gas network, respectively; $p^{\max}_{a}$, $p^{\min}_{a}$, $p^{\max}_{b}$ and $p^{\min}_{b}$ represent the upper and lower limits of the pressure at nodes a and b in the natural gas network, respectively.

c: MODEL TRANSFORMATION

Equation (15) contains nonlinear terms $G^2_{ab,n,t}$, $p^2_{a,n,t}$ and $p^2_{b,n,t}$. To facilitate solving, this paper adopts the incremental linearization method from reference [3] to transform the original nonlinear model into a mixed-integer linear programming model that can be conveniently solved, thereby greatly improving the solution efficiency. The specific linearization process is detailed in Appendix C. After linearization, Equation (15) can be represented as Equations (C5)-(C8) in Appendix C.

4) ENERGY COUPLING EQUIPMENT CONSTRAINTS

a: P2G OPERATIONAL CONSTRAINTS

$$\begin{cases} G_{u,n,t} = \eta_u P_{u,n,t} \\ M^{\mathrm{p2g}}_{k,n,t} = \sum_{u\in U} \tau^{\mathrm{CO_2}}_{u} P_{u,n,t}, \quad \forall n \in N,\ \forall t \in T \end{cases} \tag{19}$$

where η_u represents efficiency of P2G device u.

b: GAS TURBINE OPERATIONAL CONSTRAINTS

$$P_{r,n,t} = \eta_r G_{r,n,t}, \quad \forall n \in N,\ \forall t \in T \tag{20}$$

where η_r represents the efficiency of gas turbine r.

c: CHP OPERATIONAL CONSTRAINTS

$$\begin{cases} P_{c,n,t} = k_c H_{c,n,t} \\ G_{c,n,t} = \dfrac{\left(P_{c,n,t} + H_{c,n,t}\right)}{k_c}, \quad \forall n \in N,\ \forall t \in T \end{cases} \tag{21}$$

where k_c represents the efficiency of CHP unit c.

V. CASE STUDY ANALYSIS

This paper takes the E14-H6-G6 test system, consisting of a 14-node electricity grid, 6-node heating network, and 6-node gas network, as an example to validate the effectiveness of the CCS-P2G collaborative operation mode, the extended carbon emission flow model considering energy storage devices, and the PMADP algorithm. The topological diagrams of the E14-H6-G6 test systems can be found in Fig.4. The parameters of the electricity grid are referenced from the IEEE14 [30] standard models, while the parameters of the heating network and gas network are obtained from literature [27]. MATLAB with the GUROBI solver is employed for model solving. The computer configuration includes a Win10 system, Intel i5-8300H CPU with a clock speed of 3.9GHz, and 16GB of memory. The scheduling period is set to 24 hours, with each time period length being 1 hour.

A. ANALYSIS OF THE EFFECTIVENESS OF CCS-P2G COLLABORATIVE OPERATION MODE

This paper proposes the CCS-P2G collaborative operation mode, which realizes the full utilization of CO2 by constructing a conversion pathway of ‘‘emission-capture-utilization’’ for CO2. To verify the effectiveness of the proposed CCS-P2G collaborative operation mode, three scenarios are set up for comparative analysis:

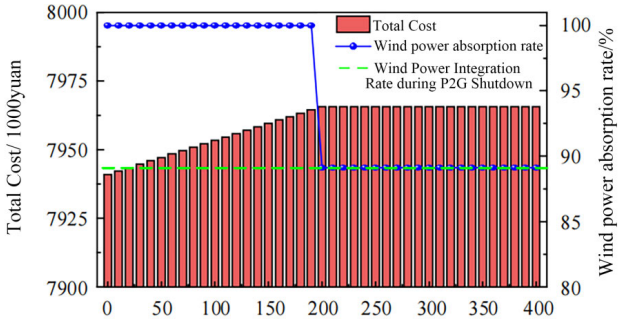

FIGURE 3. Impact of P2G Equipment Raw Material Costs on Operating Costs and Wind Power Integration Rate.

Scenario 1: No CCS retrofitting for coal-fired units.

Scenario 2: Partial CCS retrofitting for some coal-fired units, without considering the CCS-P2G collaborative operation mode.

Scenario 3: Partial CCS retrofitting for some coal-fired units, considering the CCS-P2G collaborative operation mode.

1) ANALYSIS OF P2G FEEDSTOCK COST COEFFICIENT

In Scenario 1, where no coal-fired units are considered for CCS retrofitting, P2G cannot utilize the carbon emissions from coal-fired units for methanation reaction and requires external purchase of CO2. Therefore, the feedstock cost coefficient of P2G will significantly affect the scheduling results. Hence, this paper analyzes the wind power absorption capacity and operational economy of IES under different feedstock cost coefficients for P2G. The total operating cost of IES and the wind power absorption rate with varying feedstock cost coefficients for P2G are shown in Fig.3.

From Fig.3, it can be observed that when the raw material cost of P2G is 200 yuan/(MW·h) and above, the wind power integration rate is equal to that without considering P2G equipment, both at 89.11 %. At this point, the operating cost of the Integrated Energy System (IES) is the highest, at 7.9656 million yuan. This is because when the raw material cost exceeds 200 yuan/(MW·h), the total revenue obtained from integrating wind power through P2G and generating natural gas through methanation reaction is insufficient to offset its raw material cost. Utilizing P2G equipment for wind power integration becomes uneconomical, thus P2G shuts down. As the coefficient of P2G raw material cost decreases, the economic feasibility of using P2G equipment for wind power integration increases, and the wind power integration rate rises. It can be seen that in the low-carbon dispatch of IES considering P2G equipment, the raw material cost and capacity of P2G have a significant impact on the level of wind power integration and the economic feasibility of IES operation. Therefore, this paper addresses the issue of reduced wind power integration due to insufficient P2G capacity by retrofitting coal-fired units with CCS (Carbon Capture and Storage) technology, using the energy consumption of CCS equipment to alleviate the problem. Meanwhile, coal-fired units with CCS can provide sufficient carbon raw materials for P2G equipment, effectively reducing the raw material cost of P2G equipment in the low-carbon economic dispatch of IES, making IES more economically viable in terms of low-carbon operations.

2) ANALYSIS OF DISPATCH RESULTS IN DIFFERENT SCENARIOS

To further analyze the impact of CCS retrofitting of coal-fired units on low-carbon dispatch of IES and to validate the effectiveness of the proposed CCS-P2G collaborative operation mode, the total operating costs of IES, coal-fired unit fuel costs, carbon trading costs, and P2G carbon procurement costs are compared for three different scenarios. The results are shown in Appendix B, Table 1.

From Table 1, it can be seen that in Scenario 2, based on Scenario 1, the retrofitting of coal-fired units with CCS significantly reduces carbon trading costs by 73.46%, as the carbon emissions of high-carbon-emitting coal-fired units decrease significantly. Carbon trading costs amount to 80,200 yuan. However, due to the additional operational energy consumption required by the inclusion of CCS equipment, the electricity generation costs increase by 7.85%. Additionally, carbon transportation costs increase due to the need to transport and store CO2 captured by CCS, resulting in a total cost reduction of 359,400 yuan.

In Scenario 3, based on Scenario 2, a CCS-P2G collaborative operation mode is established. In terms of carbon trading costs, further reduction is achieved by fully utilizing the CO2 captured by CCS. Under the premise of meeting carbon emission quota requirements, Scenario 3 can sell surplus carbon emission quotas in the carbon market, resulting in a profit of 59,700 yuan. Regarding carbon transportation costs and carbon procurement costs, the CCS-P2G collaborative operation mode can directly supply sufficient CO2 captured by CCS to P2G for methanation reaction, thereby reducing carbon procurement costs to zero. Consequently, the total cost decreases by 785,000 yuan compared to Scenario 2 and by 1,379,000 yuan compared to Scenario 1.

Thus, the proposed CCS-P2G collaborative operation mode, through the full reutilization of CO2, significantly improves the economic and low-carbon performance of the IES system, thereby validating the effectiveness of the CCS-P2G collaborative operation mode in low-carbon dispatch.

B. EXPANSION OF CARBON EMISSION FLOW ANALYSIS

To validate the effectiveness of the extended carbon emission flow model considering electric energy storage devices proposed in this paper, three typical periods are selected based on Scenario 3: the peak wind power output and low load period at 02:00, the low load period at 15:00, and the peak load and low wind power output period at 19:00. The carbon emission flow in the IEEE14 system is analyzed during these periods. The carbon emission flow is depicted in Appendix A, Fig.5.

From Fig.5(a) and Fig.5(d), it is evident that at 02:00, during peak wind power output and low load periods, the carbon emission flow predominantly diffuses from the 14 nodes connected to wind power across the entire network. The extended carbon emission flow model proposed in this paper accurately characterizes the carbon emission profile of electric energy storage devices. Due to the high penetration rate of wind power, the Net Carbon Intensity (NCI) of the 14 nodes connected to electric energy storage devices decreases to 0. This implies that the electric energy storage devices have effectively stored wind power, realizing the flexible utilization of low-carbon resources. Combining the analysis of the Electric Carbon Ratio (ECR) of electric energy storage devices shown in Fig.5(f), it can be inferred that the injection of low-carbon wind power reduces the ECR of electric energy storage devices while storing electricity. This effectively dilutes the high-carbon electricity stored in electric energy storage devices with low-carbon wind power, reducing the carbon emissions per unit of electricity stored. During subsequent dispatch processes, electric energy storage devices can release low-carbon electricity to meet load demand while reducing the overall NCI of the network, thereby improving the low-carbon economic efficiency of system operation.

From Fig.5(b) and Fig.5(d), it can be observed that during the low wind power output period at 15:00, the carbon emission flow predominantly diffuses from the 13 nodes connected to gas turbines throughout the entire network. Because of the low penetration rate of wind power, the proportion of output from high-carbon emitting units increases, leading to an increase in the Net Carbon Intensity (NCI) of nodes across the network compared to the peak wind power output and low load period at 02:00. The NCI of the 14 nodes connected to electric energy storage devices rises from 0 at 02:00 to 286.34 $gCO_2/(kW{\cdot}h)$ at 15:00. To ensure the power supply during subsequent peak periods and achieve globally optimal dispatch decisions, electric energy storage devices charge at 15:00. Combined with the extended carbon emission flow model, since the nodes where the electric energy storage devices are connected have an NCI (Node Carbon Intensity) not equal to zero, the electricity containing carbon emissions is stored in the electric energy storage devices. This leads to an upward trend in the ECR (Emission to Charge Ratio) of the electric energy storage devices at 15:00, as shown in Fig.5(f).

From Fig.5(c) and Fig.5(d), it can be seen that at 19:00, during the peak electric load period, the wind power penetration further decreases. To achieve globally optimal dispatch decisions, the electric energy storage devices choose to discharge. At this time, the Electric Carbon Ratio (ECR) of electric energy storage devices is 0.24 $tCO_2/(MW{\cdot}h)$. The GCI of electric energy storage devices in the discharging state is only 30% of that of coal-fired units and gas turbines. The low-carbon electricity released by electric energy storage devices is injected into the grid to some extent, reducing the Net Carbon Intensity (NCI) of certain nodes compared to the low load period at 15:00. Node 9, being close to Node 14 where electric energy storage devices are connected, has a lower NCI than at 15:00. This means that by storing wind power, the electric energy storage devices enable the flexible use of low-carbon resources, enhancing the low-carbon operation of the IES.

In summary, this paper proposes an extended carbon emission flow model and analyzes the carbon emission flow during typical periods, exploring the carbon emission characteristics of electric energy storage devices and examining the carbon emission flow paths throughout the entire source-grid-load-storage process in the IES. By flexibly coordinating renewable energy and performing charge-discharge operations in line with electricity peaks and valleys, the redistribution of low-carbon resources is achieved. The extended carbon emission flow model proposed in this paper provides effective support for low-carbon dispatching.

C. EFFECTIVENESS ANALYSIS OF PMADP ALGORITHM

Considering the multidimensional dynamic programming problem of stochastic dynamic low-carbon dispatch in IES with multiple uncertainties, there are challenges such as lengthy computation time and the ''curse of dimensionality''. In this paper, the PMADP algorithm is utilized to address these challenges by aggregating state variables, compressing state space, and employing parallel computation. While maintaining computational accuracy, the PMADP algorithm alleviates the ''curse of dimensionality''. To validate the effectiveness of the PMADP algorithm in addressing the stochastic dynamic low-carbon dispatch problem in IES with multiple uncertainties, the precision and efficiency of the traditional stochastic optimization algorithm and the serial MADP algorithm are compared with the parallel PMADP algorithm used in this study. The results are presented in Table 2 in Appendix B.

From Table 2, it can be observed that in terms of expected operating cost, the stochastic optimization algorithm achieves the lowest cost of 7.3508 million yuan by precisely solving each scenario. The traditional parallel MADP algorithm and the parallel PMADP algorithm used in this study approximate the value function to mitigate the ''curse of dimensionality'', resulting in an increase in operating cost of 0.81% compared to the stochastic optimization algorithm, both totaling 7.4102 million yuan. In terms of efficiency, the PMADP algorithm employed in this study decouples serial tasks and maximizes the utilization of computational resources through parallel computation, resulting in the shortest computation time among the three algorithms, at 408.91 seconds. This represents a 90.29% reduction compared to the stochastic optimization algorithm and a 52.58% reduction compared to the traditional serial MADP algorithm.

From a holistic perspective, although the stochastic optimization algorithm can precisely solve each scenario, its low efficiency makes it challenging to apply to the solution of large-scale systems. Compared to the stochastic optimization algorithm, the traditional serial MADP algorithm offers

some improvement in computational efficiency. However, its inefficient utilization of computational resources limits its advantages in practical engineering applications. The PMADP algorithm adopted in this study, while ensuring computational accuracy, significantly enhances computational efficiency by fully utilizing computational resources. As a result, it holds high practical value for engineering applications.

Through the above analysis, it is evident that in large-scale, multi-energy storage complex systems, the extended carbon emission flow model proposed in this paper, considering electric energy storage devices, can still accurately characterize the carbon emission flow process. It achieves ECR calculation for the entire scheduling cycle of energy storage devices, thereby clearly demonstrating the flexible utilization of low-carbon energy sources and their penetration range.

VI. CONCLUSION

This paper proposes a synergistic operation mode of Power-to-Gas with Carbon Capture and Storage (P2G-CCS), along with an extended carbon emission flow low-carbon dispatch model considering electric energy storage devices. Through case studies, the following conclusions are drawn:

1) The proposed integrated carbon emission ''generation-capture-utilization'' mode of P2G-CCS achieves full utilization of carbon emissions throughout the process compared to traditional electricity and carbon separation operation modes. This significantly improves the economic efficiency of Integrated Energy Systems (IES).
2) The proposed method for characterizing the carbon emission characteristics of electric energy storage devices tracks the carbon emission process throughout the entire scheduling cycle of electric energy storage devices. It clarifies the carbon emission responsibilities of electric energy storage devices in low-carbon dispatch, further enhancing the accuracy and rationality of low-carbon dispatch strategies for IES.
3) The proposed extended carbon emission flow model considering electric energy storage devices accurately describes the carbon emission flow process in systems with electric energy storage devices. It extends the rational assessment criteria for low-carbon dispatch strategies from the ''electricity perspective'' to the ''carbon perspective,'' providing new means for analyzing low-carbon dispatch strategies. Moreover, it demonstrates good applicability to large-scale, multi-energy storage complex systems.

Despite the significant enhancement of economic efficiency and carbon emission management precision in Integrated Energy Systems (IES) brought about by the CCS-P2G collaborative mode and the extended carbon emission flow model, limitations persist, including technological maturity, high initial investment, increased model complexity, and sensitivity to external factors. Future research should concentrate on bolstering technical feasibility, refining economic models to accurately reflect cost-benefit analyses, and delving deeper into the extended carbon emission flow model that accounts for the dynamic characteristics of heat and gas networks. Additionally, investigating the mechanisms of diversified demand-side response guided by the extended carbon emission flow will further unlock the application potential of carbon emission flow models within IES frameworks.

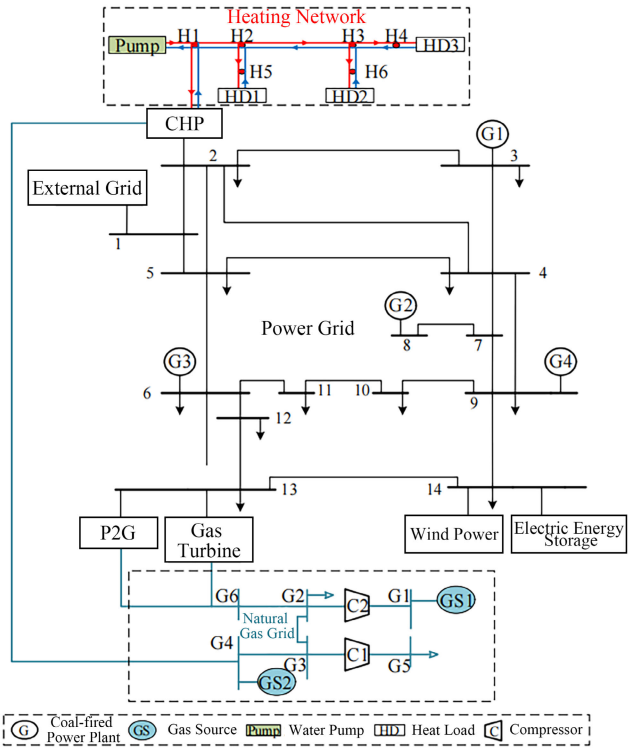

FIGURE 4. Test system of E14-H6-G6.

APPENDIX A

Fig.4 shows the topology of the E14-H6-G6 test system, Fig.5 shows the carbon emission flow model, NCI, and ECR for a typical period.

APPENDIX B

Table 1 shows the comparative results of the total operating cost of the IES, the fuel cost of coal-fired units, the carbon trading cost, and the P2G carbon purchase cost under three different scenarios. Table 2 shows a comparison of the solving accuracy and solving efficiency between traditional stochastic optimization algorithms, serial MADP algorithms, and PMADP algorithms.

APPENDIX C

The nonlinear term of the natural gas pipeline flow constraint can be expressed as $f(x) = x^2$, with the following piecewise steps:

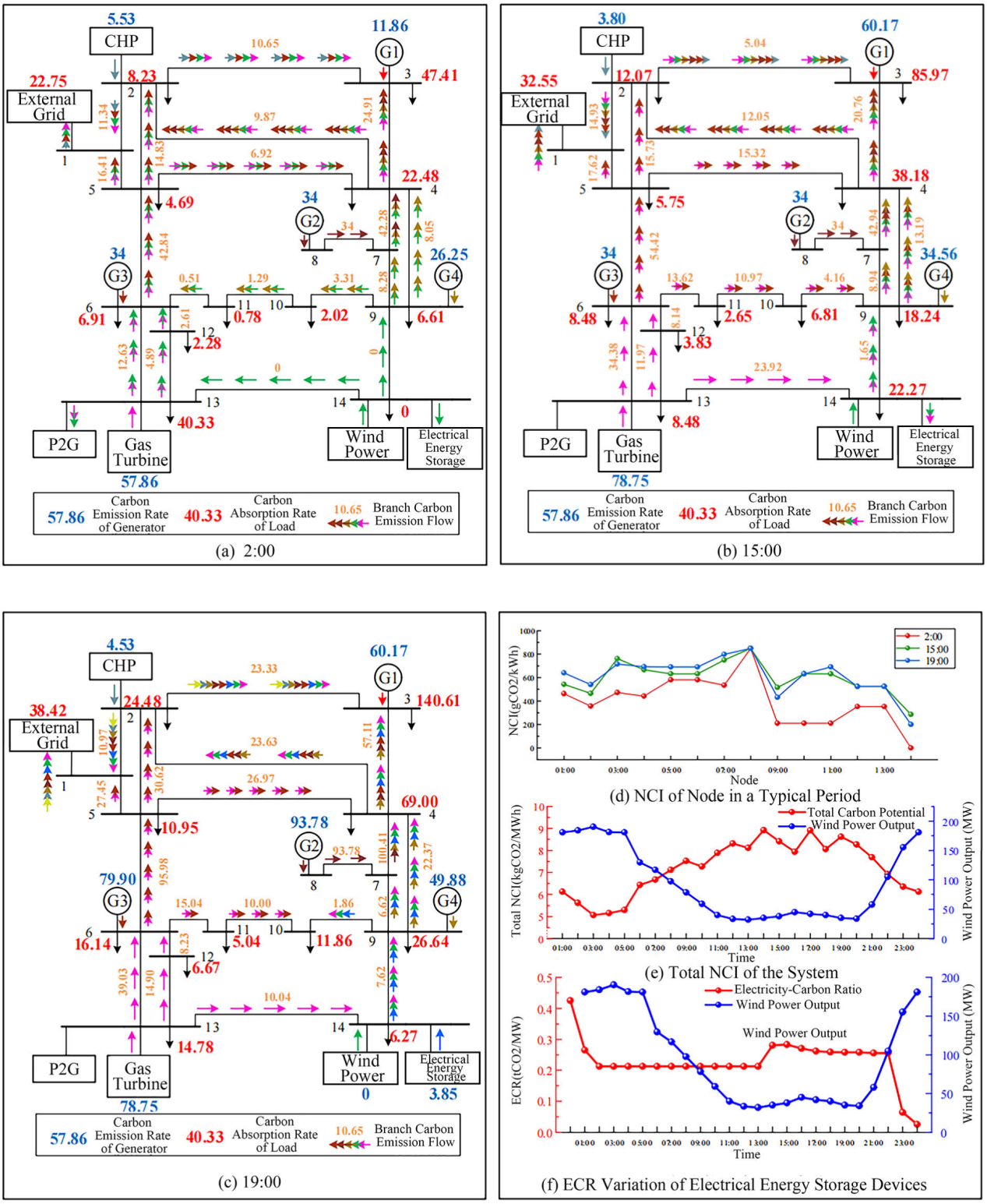

FIGURE 5. Carbon emission flow model, NCI and ECR in typical periods.

1) Select the number of segments $NP-1$;
2) Solve for the discrete points $x_1, x_2, \ldots, x_{NP}$ within the range of the independent variable;
3) Compute the function values $f(x_1), f(x_2), \ldots, f(x_{NP})$ corresponding to the discrete points $x_1, x_2, \ldots, x_{NP}$;

TABLE 1. Cost comparison of three scenarios.

Cost / (ten thousand yuan)	Scenario 1	Scenario 2	Scenario 3
Fuel cost for thermal power generation	130.78	141.05	151.43
Carbon trading cost	30.22	8.02	-5.97
Carbon transportation cost	0	4.08	3.59
P2G carbon purchase cost	0.47	1.28	0
Energy storage cost	0.24	0.31	0.30
Cost of purchased electricity	-73.25	-73.25	-73.25
Natural gas cost	656.04	657.07	654.61
Total cost	744.50	738.56	730.71

TABLE 2. Calculation results of the three algorithms.

Index	Scenario	Expected Cost/ (ten thousand yuan)	Total Time/s
Random Optimization	S1	765.21	1200.11
	S2	747.98	3403.67
	S3	735.08	4209.21
MADP	S1	766.12	554.09
	S2	747.98	754.86
	S3	741.02	862.40
PMADP	S1	766.12	280.31
	S2	747.98	365.22
	S3	741.02	408.91

4) Introduce auxiliary variables ψ and ϕ to linearize the representation of x.

$$f(x) = f(x_1) + \sum_{k=1}^{NP-1} [f(x_{k+1}) - f(x_k)]\,\psi_k \tag{C1}$$

$$x = x_1 + \sum_{k=1}^{NP-1} (x_{k+1} - x_k)\,\psi_k \tag{C2}$$

$$\psi_{k+1} \le \phi_k, \quad \phi_k \le \psi_k, \quad k = 1, 2, \cdots, N_P - 2 \tag{C3}$$

$$0 \le \psi_k \le 1, \quad k = 1, 2, \cdots, N_P - 1 \tag{C4}$$

Using the aforementioned linearization method, new linear variables $p^{\text{line}}_{a,n,t}$, $p^{\text{line}}_{b,n,t}$, and $f^{\text{line}}_{ab,n,t}$ are introduced to replace the squared terms of gas pressure and gas flow rate in equation (15). Then, equation (15) can be expressed as equation (C5):

$$f^{\text{line}}_{ab,n,t} = \left(\frac{\pi}{4}\right)^2 J_{ab} \left(p^{\text{line}}_{a,n,t} - p^{\text{line}}_{b,n,t}\right) \tag{C5}$$

According to the method described in equations (C1) to (C5), the linearization for $f^{\text{line}}_{ab,n,t}$=$G^2_{ab,n,t}$, $p^{\text{line}}_{a,n,t}$=$p^2_{a,n,t}$, and $p^{\text{line}}_{b,n,t}$=$p^2_{b,n,t}$ can be represented as follows:

$$\begin{cases} f^{\text{line}}_{ab,n,t} = \left(G^{\min}_{ab}\right)^2 + \sum_{k=1}^{NP-1} \left[G_{ab,n,t,k+1} - G_{ab,n,t,k}\right] \psi_k^{G_{ab}} \\ G_{ab,n,t} = G^{\min}_{ab} + \sum_{k=1}^{NP-1} \left(G_{ab,n,t,k+1} - G_{ab,n,t,k}\right) \psi_k^{G_{ab}} \\ \psi_{k+1}^{G_{ab}} \le \phi_k^{G_{ab}} \le \psi_k^{G_{ab}}, \quad k = 1, 2, \ldots, NP-2 \\ 0 \le \psi_k^{G_{ab}} \le 1, \quad k = 1, 2, \ldots, NP-1 \end{cases} \tag{C6}$$

$$\begin{cases} p^{\text{line}}_{a,n,t} = \left(p^{\min}_{a}\right)^2 + \sum_{k=1}^{NP-1} \left[p_{a,n,t,k+1} - p_{a,n,t,k}\right] \psi_k^{p_a} \\ p_{a,n,t} = p^{\min}_{a} + \sum_{k=1}^{NP-1} \left(p_{a,n,t,k+1} - p_{a,n,t,k}\right) \psi_k^{p_a} \\ \psi_{k+1}^{p_a} \le \phi_k^{p_a} \le \psi_k^{p_a}, \quad k = 1, 2, \ldots, NP-2 \\ 0 \le \psi_k^{p_a} \le 1, \quad k = 1, 2, \ldots, NP-1 \end{cases} \tag{C7}$$

$$\begin{cases} p^{\text{line}}_{b,n,t} = \left(p^{\min}_{b}\right)^2 + \sum_{k=1}^{NP-1} \left[p_{b,n,t,k+1} - p_{b,n,t,k}\right] \psi_k^{p_b} \\ p_{b,n,t} = p^{\min}_{b} + \sum_{k=1}^{NP-1} \left(p_{b,n,t,k+1} - p_{b,n,t,k}\right) \psi_k^{p_b} \\ \psi_{k+1}^{p_b} \le \phi_k^{p_b} \le \psi_k^{p_b}, \quad k = 1, 2, \ldots, NP-2 \\ 0 \le \psi_k^{p_b} \le 1, \quad k = 1, 2, \ldots, NP-1 \end{cases} \tag{C8}$$

APPENDIX D

A. SINGLE-INPUT SINGLE-OUTPUT ENERGY COUPLING EQUIPMENT

For single-input single-output energy coupling equipment, all carbon emissions carried by the input energy are allocated to the output energy, following the principle of carbon emission conservation: the total CEFR of the input port equals the total CEFR of the output port, which can be expressed as

$$f^{\text{PCI,in}}_{p,t} \cdot P^{\text{in}}_{p,t} = f^{\text{PCI,out}}_{p,t} \cdot P^{\text{out}}_{p,t} \tag{D1}$$

where $f^{\text{PCI,in}}_{p,t}$ and $f^{\text{PCI,out}}_{p,t}$ are the input PCI and output PCI of the energy coupling device p in the time period t, respectively; $P^{\text{in}}_{p,t}$ and $P^{\text{out}}_{p,t}$ are the input and output power of the energy coupling device p in the time period t, respectively.

If the conversion efficiency of the single-input single-output energy coupling device p is η_p, then:

$$P^{\text{out}}_{p,t} = \eta_p P^{\text{in}}_{p,t} \tag{D2}$$

Therefore, equation (D1) can be expressed as:

$$f^{\text{PCI,out}}_{p,t} = \frac{f^{\text{PCI,in}}_{p,t}}{\eta_p} \tag{D3}$$

Equation (D3) shifts the original energy conversion relationship to the carbon emission perspective, constructing the carbon emission flow model for the single-input single-output energy coupling device by utilizing the relationship between the carbon emissions at the input and output ends.

B. SINGLE-INPUT MULTIPLE-OUTPUT ENERGY COUPLING EQUIPMENT

For single-input multiple-output energy coupling equipment, the principle of carbon emission conservation still applies: all carbon emissions carried by the input energy must be allocated to the output energy. Taking a typical backpressure CHP as an example, the input natural gas energy is proportional to the output electrical energy and thermal energy, that is:

$$\begin{cases} P_{c,t} = G_{c,t}\eta_c^{\mathrm{e}} \\ H_{c,t} = G_{c,t}\eta_c^{\mathrm{h}} \end{cases} \tag{D4}$$

where $P_{c,t}$ and $H_{c,t}$ are the electrical output and thermal output of CHP unit c in the time period t, respectively; $G_{c,t}$ is the natural gas input of CHP unit c in the time period t; η_c^{e} and η_c^{h} are the electrical conversion efficiency and thermal conversion efficiency of CHP unit c in the time period t, respectively.

According to the principle of carbon emission conservation, the total CEFR at the input port equals the total CEFR at the output port:

$$f_{c,t}^{\mathrm{PCl,out}} P_{c,t} + f_{c,t}^{\mathrm{PCl,out}} H_{c,t} = f_{c,t}^{\mathrm{PCl,in}} G_{c,t} \tag{D5}$$

where $f_{c,t}^{\mathrm{PCl,out}}$ and $f_{c,t}^{\mathrm{PCl,h,out}}$ are the PCI at the electrical output port and the thermal output port of CHP unit c in the time period t, respectively; $f_{c,t}^{\mathrm{PCl,in}}$ is the PCI at the input port of CHP unit c in the time period t.

Assuming that the PCI at the electrical output port and the PCI at the thermal output port are inversely proportional to the efficiency, that is:

$$\frac{f_{c,t}^{\mathrm{PCl,out}}}{\eta_c^{\mathrm{h}}} = \frac{f_{c,t}^{\mathrm{PCl,h,out}}}{\eta_c^{\mathrm{e}}} \tag{D6}$$

Substituting equation (D6) into equation (D5) gives:

$$\begin{cases} f_{c,t}^{\mathrm{PCl,out}} = \dfrac{f_{c,t}^{\mathrm{PCl,in}}}{2\eta_c^{\mathrm{e}}} \\ f_{c,t}^{\mathrm{PCl,h,out}} = \dfrac{f_{c,t}^{\mathrm{PCl,in}}}{2\eta_c^{\mathrm{h}}} \end{cases} \tag{D7}$$

Equation (D7) is the carbon emission flow model for single-input multiple-output energy coupling equipment.

APPENDIX E

(1) Power Balance Constraints

$$\begin{aligned} &\sum_{g.\in i} P_{g,n,t} + \sum_{k.\in i} P_{k,n,t}^{\mathrm{net}} + \sum_{c.\in i} P_{c,n,t} + \sum_{r.\in i} P_{r,n,t} \\ &\quad + \sum_{w.\in i} P_{w,n,t} + \sum_{o.\in i} P_{o,n,t} + \sum_{e.\in i} P_{e,n,t}^{\mathrm{dis}} - \sum_{e.\in i} P_{e,n,t}^{\mathrm{cha}} \\ &\quad - \sum_{q.\in i} P_{q,n,t} - \sum_{u.\in i} P_{u,n,t} + \sum_{\forall b^{e}.\in i^{+}} f_{b^{e},n,t} - \sum_{\forall b^{e}.\in i^{-}} f_{b^{c},n,t} \\ &= D_{i,n,t} - P_{i,n,t}^{\mathrm{np}}, \\ &\quad \forall n \in N, \forall t \in T,\ \forall g \in G,\ \forall k \in K,\ \forall c \in C, \\ &\quad \forall r \in R, \forall w \in W,\ \forall o \in O,\ \forall e \in E,\ \forall q \in Q \end{aligned} \tag{E1}$$

where.$\in i$ indicates that the equipment is connected to the grid node i; $b^{\mathrm{e}}. \in i^{+}$ and $b^{\mathrm{e}}. \in i^{-}$ represent the branches b^{e} with the grid node i as the start and end node, respectively; $P_{q,n,t}$ is the energy consumption of the water pump q in scenario n during period t; $P_{u,n,t}$ is the electric power consumed by the P2G device u in scenario n during period t; $f_{b^{e},n,t}$ is the power flowing through the branch b^{e} in scenario n during period t; $D_{i,n,t}$ is the forecasted electrical load of node i in scenario n during period t.

(2) Operation Constraints of Coal-Fired Units with CCS

$$\begin{cases} P_{k,n,t} = P_{k,n,t}^{\mathrm{net}} + P_{k,n,t}^{\mathrm{std}} + P_{k,n,t}^{\mathrm{opt}} \\ P_{k,n,t}^{\mathrm{opt}} = \chi_k^{\mathrm{opt}} M_{k,n,t}^{\mathrm{CCS}} \\ M_{k,n,t}^{\mathrm{CCS}} = \theta_k^{\mathrm{opt}} M_{k,n,t} \\ 0 \le \theta_k^{\mathrm{opt}} \le \theta_k^{\max} \\ \qquad \forall k \in K,\ \forall t \in T,\ \forall n \in N \end{cases} \tag{E2}$$

where $P_{k,n,t}^{\mathrm{net}}$, $P_{k,n,t}^{\mathrm{std}}$, and $P_{k,n,t}^{\mathrm{opt}}$ are the net output power, fixed energy consumption, and operational energy consumption of the coal-fired unit k with CCS in scenario n during period t, respectively; χ_k^{opt} is the specific energy consumption of CCS; θ_k^{opt} and $\theta_k^{\max}$ are the carbon capture efficiency of CCS and its upper limit, respectively; $M_{k,n,t}$ is the total carbon emissions produced by the coal-fired unit k with CCS in scenario n during period t.

(3) Line Flow Constraints

$$\begin{cases} f_{ij,n,t} = \dfrac{\theta_{i,n,t} - \theta_{j,n,t}}{x_{ij}} \\ f_{ij}^{\min} \le f_{ij,n,t} \le f_{ij}^{\max} \\ \theta_i^{\min} \le \theta_{i,n,t} \le \theta_i^{\max} \\ \qquad \forall (i,j) \in L,\ \forall n \in N,\ \forall t \in T \end{cases} \tag{E3}$$

where $f_{ij,n,t}$ is the power flow through line (i,j) in scenario n during period t; $\theta_{i,n,t}$ and $\theta_{j,n,t}$ are the phase angles at nodes i and j in scenario n during period t, respectively; x_{ij} is the reactance of line (i,j); $f_{ij}^{\max}$ and $f_{ij}^{\min}$ are the upper and lower power limits of line (i,j), respectively; $\theta_i^{\max}$ and $\theta_i^{\min}$ are the upper and lower phase angle limits of node i, respectively; L is the set of lines.

(4) Operation Constraints of Energy Storage Devices

$$\begin{cases} u_{e,n,t}^{\mathrm{cha}} + u_{e,n,t}^{\mathrm{dis}} \le 1 \\ u_{e,n,t}^{\mathrm{cha}}, u_{e,n,t}^{\mathrm{dis}} \in \{0,1\} \\ 0 \le P_{e,n,t}^{\mathrm{cha}} \le u_{e,n,t}^{\mathrm{cha}} P_e^{\mathrm{cha,\,max}} \\ 0 \le P_{e,n,t}^{\mathrm{dis}} \le u_{e,n,t}^{\mathrm{dis}} P_e^{\mathrm{dis,\,max}} \\ E_{e,n,t} = E_{e,n,t-\Delta t} + \eta_e^{\mathrm{cha}} P_{e,n,t}^{\mathrm{cha}} \Delta t - \eta_e^{\mathrm{dis}} P_{e,n,t}^{\mathrm{dis}} \Delta t \\ E_e^{\min} \le E_{e,n,t} \le E_e^{\max} \\ E_{e,n,T} = E_{e,n,\mathrm{int}} \\ \forall n \in N,\ \forall t \in T \end{cases} \tag{E4}$$

where $u_{e,n,t}^{\mathrm{cha}}$ and $u_{e,n,t}^{\mathrm{dis}}$ are binary variables representing the charging and discharging states of the electric energy storage device e in scenario n during period t, respectively; $P_e^{\mathrm{cha,\,max}}$ and $P_e^{\mathrm{dis,\,max}}$ are the maximum charging and discharging

power of the electric energy storage device e, respectively; η_e^{cha} and η_e^{dis} are the charging and discharging efficiencies of the electric energy storage device e, respectively; $E_e^{\min}$ and $E_e^{\max}$ are the minimum and maximum usable capacities of the electric energy storage device e, respectively; $E_{e,n,T}$ and $E_{e,n,\text{int}}$ are the usable capacities of the electric energy storage device e at the end and the beginning of the scheduling period in scenario n, respectively.

(5) Unit Operating Limits and Ramp Rate Constraints

$$\begin{cases} P_g^{\min} \le P_{g,n,t} \le P_g^{\max} \\ P_k^{\min} \le P_{k,n,t} \le P_k^{\max} \\ P_r^{\min} \le P_{r,n,t} \le P_r^{\max} \\ P_c^{\min} \le P_{c,n,t} \le P_c^{\max} \end{cases} \quad \forall g \in G,\ \forall k \in K,\ \forall r \in R, \quad \forall c \in C,\ \forall n \in N,\ \forall t \in T \tag{E5}$$

$$\begin{cases} -r_g^{\text{down}} \le P_{g,n,t} - P_{g,n,t-\Delta t} \le r_g^{\text{up}} \\ -r_k^{\text{down}} \le P_{k,n,t} - P_{k,n,t-\Delta t} \le r_k^{\text{up}} \\ -r_r^{\text{down}} \le P_{r,n,t} - P_{r,n,t-\Delta t} \le r_r^{\text{up}} \\ -r_c^{\text{down}} \le P_{c,n,t} - P_{c,n,t-\Delta t} \le r_c^{\text{up}} \end{cases} \quad \forall g \in G,\ \forall k \in K,\ \forall r \in R, \quad \forall c \in C,\ \forall n \in N,\ \forall t \in T \tag{E6}$$

where $P_g^{\max}/P_g^{\min}$, $P_k^{\max}/P_k^{\min}$, $P_r^{\max}/P_r^{\min}$, and $P_c^{\max}/P_c^{\min}$ are the upper and lower output limits for coal-fired unit g, coal-fired unit with CCS k, gas turbine r, and CHP unit c, respectively; $r_g^{\text{up}}/r_g^{\text{down}}$, $r_k^{\text{up}}/r_k^{\text{down}}$, $r_r^{\text{up}}/r_r^{\text{down}}$, and $r_c^{\text{up}}/r_c^{\text{down}}$ are the upward/downward ramp rates for coal-fired unit g, coal-fired unit with CCS k, gas turbine r, and CHP unit c, respectively.

APPENDIX F

$$\text{NCI}_{z,t}^{\text{h}} = \frac{\sum_{b^{\text{h}}.\in t^+} f_{b^{\text{h}},t}^{\text{h}} \cdot \text{BCI}_{b^{\text{h}},t}^{\text{h}} + \sum_{c.\in z} H_{c,t} \cdot \text{GCI}_{c,t}^{\text{h}}}{\sum_{b^{\text{h}}.\in t^+} f_{b^{\text{h}},t}^{\text{h}} + \sum_{c.\in z} H_{c,t}} \tag{F1}$$

$$\text{NCI}_{a,t}^{\text{g}} = \frac{\sum_{b^{\text{g}}.\in a^+} f_{b^{\text{g}},t}^{\text{g}} \cdot \text{BCI}_{b^{\text{g}},t}^{\text{g}} + \sum_{s.\in a} G_{s,t} \cdot \text{GCI}_{s,t}}{\sum_{b^{\text{g}}.\in a^+} f_{b^{\text{g}},t}^{\text{g}} + \sum_{s.\in a} G_{s,t}} \tag{F2}$$

where $\text{NCI}_{z,t}^{\text{h}}$ and $\text{NCI}_{a,t}^{\text{g}}$ are the NCI of thermal system node z and natural gas system node a during period t, respectively; $f_{b^{\text{h}},t}^{\text{h}}$ and $f_{b^{\text{g}},t}^{\text{g}}$ are the thermal flow through the thermal system pipeline b^{h} and the gas flow through the natural gas system pipeline b^{g} with node z and node a as the starting node during period t, respectively; $\text{BCI}_{b^{\text{h}},t}^{\text{h}}$ and $\text{BCI}_{b^{\text{g}},t}^{\text{g}}$ are the BCI of the thermal system pipeline b^{h} and the natural gas system pipeline b^{g} during period t, respectively; $H_{c,t}$ and $G_{s,t}$ are the thermal power of CHP unit c' and the gas flow of gas source s during period t, respectively; $\text{GCI}_{c,t}$ and $\text{GCI}_{s,t}$ are the GCI of CHP unit c and gas source s, respectively.

REFERENCES

[1] Y. Yu, X. Han, M. Yang, and J. Yang, "Probabilistic prediction of regional wind power based on spatiotemporal quantile regression," *IEEE Trans. Ind. Appl.*, vol. 56, no. 6, pp. 6117–6127, Nov. 2020.
[2] Z. Si, M. Yang, Y. Yu, and T. Ding, "Photovoltaic power forecast based on satellite images considering effects of solar position," *Appl. Energy*, vol. 302, Nov. 2021, Art. no. 117514.
[3] J. Fan, Z. Meng, M. Shan, and L. Lv, "A review of key technologies and international standardization of multi energy coupling systems," *Power Syst. Clean Energy*, vol. 39, no. 12, pp. 1–9, 2023.
[4] X. Chen, M. B. McElroy, and C. Kang, "Integrated energy systems for higher wind penetration in China: Formulation, implementation, and impacts," *IEEE Trans. Power Syst.*, vol. 33, no. 2, pp. 1309–1319, Mar. 2018.
[5] Y. Zhang, Y. Han, D. Liu, and X. Dong, "Low-carbon economic dispatch of electricity-heat-gas integrated energy systems based on deep reinforcement learning," *J. Modern Power Syst. Clean Energy*, vol. 11, no. 6, pp. 1–14, 2023.
[6] Z. Li, L. Wu, Y. Xu, S. Moazeni, and Z. Tang, "Multi-stage real-time operation of a multi-energy microgrid with electrical and thermal energy storage assets: A data-driven MPC-ADP approach," *IEEE Trans. Smart Grid*, vol. 13, no. 1, pp. 213–226, Jan. 2022.
[7] Z. Zhang, C. Wang, S. Chen, Y. Zhao, X. Dong, and X. Han, "Multitime scale co-optimized dispatch for integrated electricity and natural gas system considering bidirectional interactions and renewable uncertainties," *IEEE Trans. Ind. Appl.*, vol. 58, no. 4, pp. 5317–5327, Jul. 2022.
[8] X. Shi, J. Feng, F. Zhang, and C. Guo, "Optimal scheduling of electrical-gas coupling system considering dynamic gas flow," in *Proc. Tsinghua-IET Elect. Eng. Academic Forum*, 2023, pp. 50–57.
[9] Z. Li, F. Zhang, J. Liang, Z. Yun, and J. Zhang, "Optimization on microgrid with combined heat and power system," in *Proc. CSEE*, Jul. 2015, pp. 3569–3576.
[10] W. Wang, S. Huang, G. Zhang, J. Liu, and Z. Chen, "Optimal operation of an integrated electricity-heat energy system considering flexible resources dispatch for renewable integration," *J. Modern Power Syst. Clean Energy*, vol. 9, no. 4, pp. 699–710, Jul. 2021.
[11] D. Xu, Q. Wu, B. Zhou, C. Li, L. Bai, and S. Huang, "Distributed multi-energy operation of coupled electricity, heating, and natural gas networks," *IEEE Trans. Sustain. Energy*, vol. 11, no. 4, pp. 2457–2469, Oct. 2020.
[12] Z. Zhang, C. Wang, H. Lv, F. Liu, H. Sheng, and M. Yang, "Day-ahead optimal dispatch for integrated energy system considering Power-to-gas and dynamic pipeline networks," *IEEE Trans. Ind. Appl.*, vol. 57, no. 4, pp. 3317–3328, Jul. 2021.
[13] J. Zhang, X. Wang, C. Jiang, K. Gong, S. Yin, and M. Yang, "Two-stage robust optimal scheduling of distribution network containing cogeneration units in new towns," *Automat. Electr. Power Syst.*, vol. 43, no. 23, pp. 155–163, 2019.
[14] Y. Liu and T. Liu, "Research on system planning of gas-power integrated system based on improved two-stage robust optimization and non-cooperative game method," *IEEE Access*, vol. 9, pp. 79169–79181, 2021.
[15] Z. Yan, C. Li, Y. Yao, W. Lai, J. Tang, C. Shao, and Q. Zhang, "Bi-level carbon trading model on demand side for integrated electricity-gas system," *IEEE Trans. Smart Grid*, vol. 14, no. 4, pp. 2681–2696, Jul. 2022.
[16] W. Liao, D. Liu, Y. Wu, and J. Weng, "Low-carbon economic dispatch of power system considering source-load uncertainties and users response behavior," in *Proc. CSEE*, Feb. 2024, pp. 905–918.
[17] N. Yan, G. Ma, X. Li, and J. M. Guerrero, "Low-carbon economic dispatch method for integrated energy system considering seasonal carbon flow dynamic balance," *IEEE Trans. Sustain. Energy*, vol. 14, no. 1, pp. 576–586, Jan. 2023.
[18] A. Akbari-Dibavar, B. Mohammadi-Ivatloo, K. Zare, T. Khalili, and A. Bidram, "Economic-emission dispatch problem in power systems with carbon capture power plants," *IEEE Trans. Ind. Appl.*, vol. 57, no. 4, pp. 3341–3351, Jul. 2021.
[19] X. Liu, X. Li, J. Tian, G. Yang, H. Wu, R. Ha, and P. Wang, "Low-carbon economic dispatch of integrated electricity-gas energy system considering carbon capture, utilization and storage," *IEEE Access*, vol. 11, pp. 25077–25089, 2023.
[20] B. Qiu, Z. Gao, and K. Wang, "IES low-carbon economic dispatch considering natural gas pressure energy power generation under P2G-CCS," in *Proc. IEEE Int. Conf. Power Sci. Technol. (ICPST)*, May 2023, pp. 793–800.

[21] Y. Li, W. Tang, and Q. Wu, "Modified carbon trading based low-carbon economic dispatch strategy for integrated energy system with CCHP," in *Proc. IEEE Milan PowerTech*, Jun. 2019, pp. 1–6.
[22] Y. Cheng, N. Zhang, B. Zhang, C. Kang, W. Xi, and M. Feng, "Low-carbon operation of multiple energy systems based on energy-carbon integrated prices," *IEEE Trans. Smart Grid*, vol. 11, no. 2, pp. 1307–1318, Mar. 2020.
[23] J. Chen, J. Zhu, W. Liu, L. Fang, and M. Liu, "MADP-based explicit online operation policy for robust energy management of ADN," *IEEE Trans. Smart Grid*, vol. 15, no. 4, pp. 3795–3807, Jul. 2024, doi: 10.1109/TSG.2024.3371221.
[24] C. Kang, T. Zhou, Q. Chen, J. Wang, Y. Sun, Q. Xia, and H. Yan, "Carbon emission flow from generation to demand: A network-based model," *IEEE Trans. Smart Grid*, vol. 6, no. 5, pp. 2386–2394, Sep. 2015.
[25] H. Chen, W. Mao, R. Zhang, and W. Yu, "Low-carbon operation of multiple energy systems based on energy-carbon integrated prices," *IEEE Trans. Smart Grid*, vol. 11, no. 2, pp. 1307–1318, Mar. 2020.
[26] Y. Cheng, N. Zhang, Y. Wang, J. Yang, C. Kang, and Q. Xia, "Modeling carbon emission flow in multiple energy systems," *IEEE Trans. Smart Grid*, vol. 10, no. 4, pp. 3562–3574, Jul. 2019.
[27] Y. Zhang, P. Zhang, X. Ji, M. Yang, Y. Yu, and X. Zhang, "Low-carbon operation of multiple energy systems based on energy-carbon integrated prices," *Autom. Electric Power Syst.*, vol. 47, no. 4, pp. 60–68, 2023.
[28] Y. Zhang, X. Zhang, X. Ji, X. Han, C. Wang, and Y. Yu, "Synergetic unit commitment of transmission and distribution network considering dynamic characteristics of electricity-gas-heat integrated energy system," in *Proc. CSEE*, 2022, pp. 8576–8591.
[29] Y. Cui, C. Gu, X. Fu, G. Deng, Y. Zhao ,and Y. Tang, "Low-carbon economic dispatch of integrated energy system with carbon capture power plants considering generalized electric heating demand response," in *Proc. CSEE*, 2022, pp. 8431–8445.
[30] W. Xunjie, L. Bowen, Z. Hainan, W. Chengfu, S. Donglei, and L. Zhe, "Optimal planning method of IES with multi-energy storage and wind power," in *Proc. IEEE Sustain. Power Energy Conf.*, Nov. 2019, pp. 2869–2872.

LIXIA WANG is currently a Senior Economist with State Grid Liaoning Electric Power Company Ltd. Her research interest includes data management.

HAODONG ZHAO received the Master of Engineering degree. He is currently a Senior Engineer with State Grid Shenyang Electric Power Supply Company, specializing in research in the fields of big data applications, the Internet of Things in power systems, and enterprise informatization.

DAWEI WANG received the Master of Engineering degree. He is currently a Senior Engineer with State Grid Liaoning Electric Power Company Ltd. His main research interest includes network security.

FANG DONG received the Master of Engineering degree. She is currently a Senior Engineer with the State Grid Liaoning Electric Power Research Institute. Her primary research interests include electrical engineering and automation.

TIANMIN FENG received the Master of Engineering degree. He is currently a Senior Engineer with State Grid Shenyang Electric Power Supply Company, with a primary research interests include power systems and automation.

RUI XIONG is currently an Engineer with State Grid Shenyang Electric Power Supply Company. His primary research interests include electrical engineering and automation.